# The effect of CO–H2O collisions in the rotational excitation of cometary CO

A Faure, François Lique, J Loreau

Monthly Notices
of the
ROYAL ASTRONOMICAL SOCIETY

MNRAS **493,** 776–782 (2020)
Advance Access publication 2020 January 25

doi:10.1093/mnras/staa242

# The effect of CO−$H_2O$ collisions in the rotational excitation of cometary CO

A. Faure [1]★ F. Lique [2]★ and J. Loreau [3]★

[1] *CNRS, IPAG, Université Grenoble Alpes, F-38000 Grenoble, France*
[2] *LOMC, Normandie Université, Université du Havre and CNRS, F-76063 Le Havre, France*
[3] *KU Leuven, Department of Chemistry, B-3001 Heverlee, Belgium*

Accepted 2020 January 20. Received 2020 January 15; in original form 2019 December 10

## ABSTRACT

We present the first accurate rate coefficients for the rotational excitation of CO by $H_2O$ in the kinetic temperature range 5–100 K. The statistical adiabatic channel method (SACM) is combined with a high-level rigid-rotor CO−$H_2O$ intermolecular potential energy surface. Transitions among the first 11 rotational levels of CO and the first 8 rotational levels of both *para*-$H_2O$ and *ortho*-$H_2O$ are considered. Our rate coefficients are compared to previous data from the literature and they are also incorporated in a simple non-LTE model of cometary coma including collision-induced transitions, solar radiative pumping and radiative decay. We find that the uncertainties in the collision data have significant influence on the CO population distribution for $H_2O$ densities in the range $10^3$–$10^8$ cm$^{-3}$. We also show that the rotational distribution of $H_2O$ plays an important role in CO excitation (owing to correlated energy transfer in both CO and $H_2O$), while the impact of the ortho-to-para ratio of $H_2O$ is found to be negligible.

**Key words:** molecular data – molecular processes – scattering – comets: general.

## 1 INTRODUCTION

Rate coefficients (or cross sections) for molecular collisional excitation are needed to model both thermal balance and spectral line formation in astrophysical objects such as interstellar clouds, protoplanetary discs, and planetary/cometary atmospheres. In such environments, the density can be so low ($n \ll 10^{10}$ cm$^{-3}$) that collisions indeed cannot maintain a local thermodynamical equilibrium (LTE) everywhere. Until recently, the accuracy of theoretical collision data was mainly inferred indirectly by comparison with related processes such as line broadening cross-sections (see e.g. Mengel, Flatin & De Lucia 2000; Wiesenfeld & Faure 2010). In the last decade, there has been huge progress in measuring state-to-state collision cross-sections at very low energy ($E_{\rm col} \sim 1$ meV) (see Naulin & Bergeat 2018, for a recent review). Detailed comparisons between quantum calculations and crossed -beam measurements have thus allowed experimentalists to verify theoretical cross-sections in the 'cold' regime (equivalent temperature ∼10 K) where quantum effects such as resonances are predominant. Theory has passed all experimental tests so far, establishing the reliability of modern collisional data used in astrophysical models (Chefdeville et al. 2013, 2015; Bergeat et al. 2020; Gao et al. 2019). These theoretical values have been obtained for 'simple' collision systems such as rigid rotors excited by light atomic or diatomic perturbers, in particular He atoms and $H_2$ molecules which are the most abundant collisional partners in the interstellar medium (ISM).

However, collision rate coefficients are also needed for systems involving heavy and even polyatomic perturbers, which challenge current computational capabilities. For instance, in the thermosphere of Titan, $N_2$, and $CH_4$ are the most abundant collisional perturbers (Rezac et al. 2013). In cometary comas, collisional excitation is generally dominated by $H_2O$ (and/or electrons) and, for comets at large heliocentric distances, by CO (Bockelée-Morvan et al. 2004). The main difficulty with such systems is the excessively large number of angular couplings between the target and the projectile which make full quantum calculations prohibitively expensive, both in terms of computer time and memory requirements. As a result, to the best of our knowledge, the only sets of rotationally resolved rate coefficients for the water perturber are those of Green (1993) for CO−$H_2O$, those of Buffa et al. (2000) for $H_2O$−$H_2O$, and those of Dubernet & Quintas-Sánchez (2019) for HCN−$H_2O$. The two former sets were estimated using crude treatments while the latter was obtained using only partially converged coupled-states (CS) calculations.

In this paper, we present the first quantum calculations for the rotational excitation of CO by $H_2O$ molecules. This is also the first study to consider the two nuclear-spin isomers of $H_2O$, *ortho*-, and *para*-$H_2O$ (hereafter referred as o-$H_2O$ and p-$H_2O$), as two distinct perturbers. The statistical adiabatic channel model (SACM) is used as a validated alternative to prohibitive close-coupling calculations

★ E-mail: alexandre.faure@univ-grenoble-alpes.fr (AF); francois.lique@univ-lehavre.fr (FL); jerome.loreau@kuleuven.be (JL)

(Loreau, Lique & Faure 2018a, 2018b) and it is combined here with the recent ab initio CO−$H_2O$ interaction potential computed by Kalugina et al. (2018). The CO−$H_2O$ collision system is of great importance in comets but also in protoplanetary and debris discs when the gas originates from ices in planetesimals (Matrà et al. 2015). In addition to providing collision data for the first 11 rotational levels of CO, we also present a non-LTE model for the CO excitation in comets, including collision-induced transitions due to p-$H_2O$ and o-$H_2O$, radiative pumping of the $v = 0 \rightarrow 1$ band due to solar photons and radiative decay due to spontaneous emission. A key objective is to assess the impact of accurate CO−$H_2O$ collisional data on the rotational distribution of cometary CO. The next section describes the CO−$H_2O$ scattering calculations. Section 3 compares the present results with previous collisional data for CO. In Section 4, we present simple non-equilibrium calculations for the excitation of CO in comets. Concluding remarks are made in Section 5.

## 2 QUANTUM STATISTICAL CALCULATIONS

The computation of inelastic cross-sections from first principles consists of two main steps. First, the electronic Schrödinger equation is solved using quantum chemistry methods. Within the Born–Oppenheimer approximation, a single intermolecular potential energy surface (PES) governing the motion of the nuclei is defined as function of nuclear coordinates. The nuclear motion is solved separately, in a second step, using quantum or (semi)classical scattering methods. We describe in this section our calculations for the CO−$H_2O$ system.

### 2.1 Potential energy surface

The CO−$H_2O$ scattering calculations presented below are based on the high-level ab initio intermolecular potential recently determined by Kalugina et al. (2018). The interacting molecules CO and $H_2O$ are considered as rigid-rotors, with geometries corresponding to their ground vibrational state. The PES was calculated at 93 000 relative orientations using the explicitly correlated single- and double-excitation coupled cluster theory with a non-iterative perturbative treatment of triple excitations [CCSD(T)-F12a] along with the augmented correlation-consistent aug-cc-pVTZ basis sets (AVTZ hereafter). The intermolecular energies were then fitted to a body-fixed expansion expressed as a sum of spherical harmonic products and a Monte Carlo estimator was employed to select the largest expansion terms. This CO−$H_2O$ PES has a global well depth $D_e = 646.1$ cm$^{-1}$ for an intermolecular centre-of-mass separation $R = 7.42\ a_0$ and a planar configuration OC−$H_2O$, with a weak hydrogen bond between the C atom of CO and one H atom of $H_2O$. Bound-state rovibrational energy calculations using this PES have been found in very good agreement with experiments (Barclay et al. 2019), confirming the good accuracy of the potential. We note that a full-dimensional CO−$H_2O$ PES was recently computed at the same level (CCSD(T)-F12a/AVTZ) by Liu & Li (2019). These authors found a similar but deeper well depth ($D_e = 685.5$ cm$^{-1}$), which is due to the basis set superposition error (BSSE) not corrected by Liu & Li (2019).

### 2.2 The statistical adiabatic channel model

Rigourous close-coupling quantum scattering calculations become impracticable when the number of coupled channels exceed typically 10 000. In such situation, statistical methods may provide a useful alternative. Statistical theories generally apply when a collisional system can access a deep well on the PES and the lifetime of the complex is sufficiently long. We have recently (Loreau et al. 2018a) developed a statistical approach inspired by the SACM of Quack & Troe (1975). In our implementation, we diagonalize the Hamiltonian excluding the kinetic term in the basis of rotational functions for the collision. In this case, the angular functions are products of Wigner rotation matrices for $H_2O$ and spherical harmonics for CO as well as for the relative orbital motion (Phillips, Maluendes & Green 1995). This expansion corresponds to the coupling of the angular momenta $\boldsymbol{j}_1$ of $H_2O$, $\boldsymbol{j}_2$ of CO, and $\boldsymbol{\ell}$ for the relative motion to form the total angular momentum $\boldsymbol{J} = \boldsymbol{j_1} + \boldsymbol{j_2} + \boldsymbol{\ell}$. Upon diagonalization, for each value of $J$ we obtain a set of adiabatic rotational curves as a function of the intermolecular distance $R$ with an asymptotic value given by the sum of rotational energies of $H_2O$ and CO. These curves possess centrifugal barriers that depend on the orbital quantum number $\ell$, and for a given initial state, the collision is assumed to take place if the collision energy is larger than the height of the barrier. The probability is then divided equally among the channels for which the energy is larger than their respective centrifugal barriers, allowing us to compute state-to-state cross-sections and rate coefficients.

This procedure was found to provide rate coefficients with an average accuracy better than 50 per cent for ion–molecule systems up to room temperature (Loreau et al. 2018a). In the case of CO−$H_2O$, the SACM *partial* rate coefficients (computed for a total angular momentum $J = 0$) were shown to be accurate to within 40 per cent up to 100 K (Loreau et al. 2018b). Full comparisons between SACM and close-coupling calculations can be found in the two papers by Loreau and co-workers.

In this paper, the cross-sections were calculated for transitions among the first 11 energy levels of CO (up to $j_2 = 10$) and the first 8 energy levels of both p-$H_2O$ and o-$H_2O$ (up to $j_1 = 3$) and for collision energies between 0 and 500 cm$^{-1}$ in order to derive rate coefficients up to $T = 100$ K. This requires to obtain all the adiabatic curves up to a total energy of 750 cm$^{-1}$. The basis set of angular functions included levels up to $j_1 = 5$ and $j_2 = 15$, and tests were performed to ensure the convergence of the adiabatic curves with respect to the size of the basis set. The rotational constant of CO was taken to be $B_0 = 1.92253$ cm$^{-1}$, while the energy of the rotational levels of $H_2O$, $E_{j_1 k_a k_c}$, was obtained using the effective Hamiltonian of Kyrö (1981). They are labelled with $j_1$, $k_a$, and $k_c$, where $k_a$ and $k_c$ are pseudo-quantum numbers corresponding to the projection of the angular momentum $j_1$ along the axis of least and greatest moment of inertia, respectively. Adiabatic curves were generated for values of the total angular momentum from $J = 0$ up to $J = 100$ for o-$H_2O$ and p-$H_2O$ separately. High total angular momentum values were found to be necessary as the cross-section converges very slowly with $J$ due to the deep well in the PES as well as to the large reduced mass of $H_2O$–CO.

Two sets of rate coefficients describing the excitation of CO by $H_2O$ were considered: the first consists of rate coefficients for which $H_2O$ is in the ground rotational state of its nuclear-spin isomer, i.e. $k_{j_2 \rightarrow j_2'}(T) = k_{0_{00}, j_2 \rightarrow 0_{00}, j_2'}(T)$ or $k_{1_{01}, j_2 \rightarrow 1_{01}, j_2'}(T)$ for p-$H_2O$ and o-$H_2O$, respectively. This set of 'ground-state' rate coefficients neglects the simultaneous excitation of CO and $H_2O$ as well as the fact that excited rotational states of $H_2O$ can be significantly populated. Such an approximation is therefore expected to be accurate only at very low temperatures.

To take into account the transitions in $H_2O$, we constructed a second set of rate coefficients (separately for p-$H_2O$ and o-$H_2O$) by summing over all possible final states of $H_2O$, and averaging over

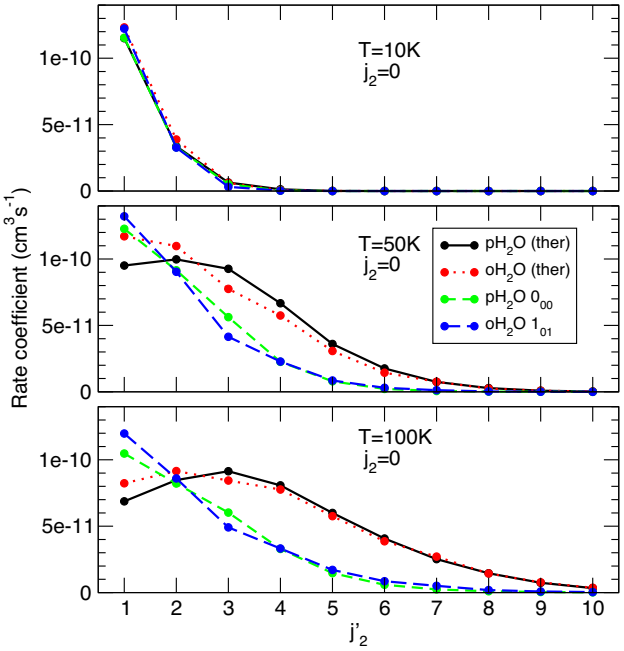


**Figure 1.** SACM rate coefficients for the rotational excitation of CO by $H_2O$ from the ground state ($j_2 = 0$) to the lowest 10 excited states. The projectiles p-$H_2O$ and o-$H_2O$ are assumed to be either thermalized at the kinetic temperature (10, 50, or 100 K) or in their ground rotational states $0_{00}$ and $1_{01}$, respectively. See text for details.

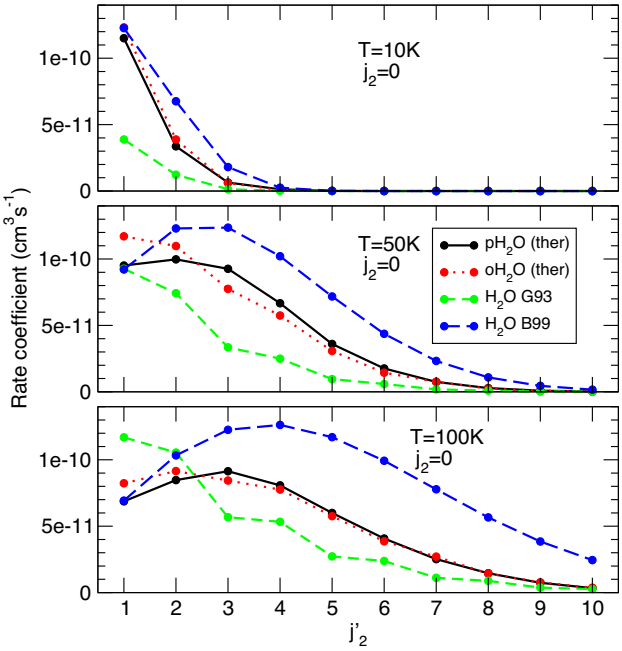


**Figure 2.** Same as Fig. 1. The thermalized SACM data for p-$H_2O$ and o-$H_2O$ are compared to the data of Biver et al. (1999) and Green (1993). See text for details.

the initial rotational states of $H_2O$ assuming a thermal population distribution:

$$k_{j_2 \to j_2'}(T) = \sum_{j_1 k_a k_c j_1' k_a' k_c'} P_{j_1 k_a k_c}(T) k_{j_1 k_a k_c, j_2 \to j_1' k_a' k_c', j_2'}(T), \quad (1)$$

where

$$P_{j_1 k_a k_c}(T) = \frac{g_{j_1} \exp(-E_{j_1 k_a k_c}/k_B T)}{\sum_{j_1 k_a k_c} g_{j_1} \exp(-E_{j_1 k_a k_c}/k_B T)} \quad (2)$$

is the Boltzmann population of level $j_1 k_a k_c$ at temperature $T$ and $k_B$ is the Boltzmann constant. This set of 'thermalized' rate coefficients assumes that the kinetic and rotational temperatures are equal, and satisfies detailed balance. These thermalized rate coefficients can be much larger than the ground-states values, even at low temperature, owing to correlated rotational energy transfer in both collision partners (see below). All de-excitation rate coefficients are available as supplementary material. Excitation rate coefficients can be derived using the detailed balance principle.

## 3 RESULTS

Rate coefficients for the rotational excitation of CO by $H_2O$ are presented below at three kinetic temperatures, 10, 50, and 100 K, for transitions out of the ground rotational state of CO ($j_2 = 0$) as functions of the final $j_2$ ($j_2' = 1$–10). In Fig. 1, four sets of data are presented, corresponding to the 'ground-state' and 'thermalized' SACM rate coefficients defined above with p-$H_2O$ and o-$H_2O$ as colliders. It is seen that all four sets have very similar rate coefficients at 10 K and that the transition $j_2 = 0 \to 1$ dominates. Small differences between thermalized and ground-state rate coefficients were expected at 10 K because (i) only the ground-state of p-$H_2O$ and o-$H_2O$ is significantly populated at thermal equilibrium and (ii) the excitation of $H_2O$ is inhibited because the rotational thresholds are larger than 10 K (23 and 54 K for the first excitation in o-$H_2O$ and p-$H_2O$, respectively). In fact, however, substantial differences (more than a factor of 2) are found for transitions with $j_2' > 3$ whose rate coefficients are smaller than $10^{-11}$ cm$^3$ s$^{-1}$. For instance, the thermalized and ground-state rate coefficients for the excitation $j_2 = 0 \to 4$ ($\Delta E = 38.4$ cm$^{-1}$) by p-$H_2O$ are $1.26 \times 10^{-12}$ and $3.16 \times 10^{-13}$ cm$^3$ s$^{-1}$, respectively. The much larger thermalized value is due to the correlation between the CO excitation $j_2 = 0 \to 4$ ($\Delta E = 38.4$ cm$^{-1}$) and the simultaneous $H_2O$ de-excitation $j_1 k_a k_c = 1_{11} \to 0_{00}$ ($\Delta E = 37.1$ cm$^{-1}$). This particular process provides a major contribution to the thermalized rate coefficient, despite the low population of the $1_{11}$ level at 10 K ($\sim$1 per cent). We also note that the near-resonant character of this correlated (de)excitation is not accounted for by SACM calculations and that close-coupling calculations would predict an even larger thermalized rate coefficient. At 50 and 100 K, the differences between the thermalized and the ground-state rate coefficients are clearly visible, reflecting both the larger population of excited $H_2O$ levels (thus pair correlations) and the opening of excitation channels in $H_2O$. In particular, the transitions $j_2 = 0 \to 2, 3$ are preferred in the thermalized data at 100 K while $j_2 = 0 \to 1$ is favoured in the ground-state data. We also note that the difference between p-$H_2O$ and o-$H_2O$ is very small, both for thermalized and ground-state data, suggesting that the ortho-to-para ratio (OPR) of $H_2O$ should not play a major role in the excitation of CO (see Section 4 below).

In Fig. 2, the above set of thermalized rate coefficients is compared to previous data from the literature: those of Biver et al. (1999) (denoted as B99) and those of Green (1993) (denoted as G93). Biver et al. (1999) assumed a *total* cross-section of $\sigma_c = 2 \times 10^{-14}$ cm$^{-2}$, with no energy dependence. This value was derived from room temperature pressure broadening measurements on $H_2O$–$H_2O$ (Biver 1997), with an estimated uncertainty of a factor of $\sim$2. The total collisional rate coefficient was computed as $k_c(T) = \sigma_c \langle v(T) \rangle$, where $T$ is the kinetic temperature and $\langle v(T) \rangle$ is the thermal mean velocity of the CO molecule relative to the

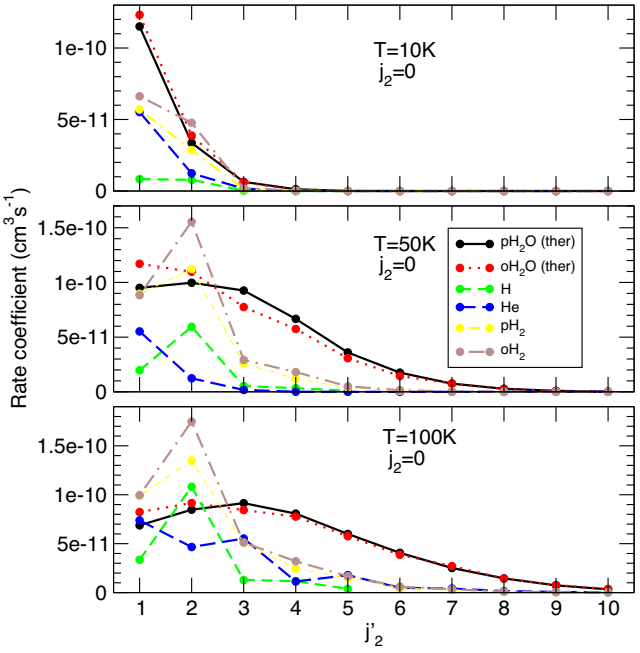


**Figure 3.** Same as Fig. 1. The thermalized SACM data for p-$H_2O$ and o-$H_2O$ are compared to the data for other projectiles: H, He, p-$H_2$, and o-$H_2$.

cometary gas. State-to-state rate coefficients from an initial CO level $j_2$ to a final level $j_2'$ were then obtained as $k_{j_2 \to j_2'}(T) = k_c P_{j_2'}(T)$, where $P_{j_2'}(T)$ is the Boltzmann population of the final level $j_2'$ at temperature $T$. This recipe corresponds to assuming that each collision redistributes the molecule according to the Boltzmann distribution, which has no physical basis, except that it satisfies the detailed balance principle (by construction). Green (1993), on his side, combined line shape measurements on $N_2$–$H_2O$ with a rate-law derived from the infinite-order-sudden (IOS) approximation. The total excitation rates were expected to be rather accurate (about 10 per cent) at room temperature, where the rate-law parameters were fitted. It should be noted that in contrast to our SACM calculations, the B99 and G93 collision data sets do not distinguish between p-$H_2O$ and o-$H_2O$. It is found in Fig. 2 that the magnitude and the $\Delta j_2 = j_2' - j_2$ dependence of the rate coefficients are reasonably described by the B99 and G93 data sets: the largest rate coefficients are $\sim 10^{-10}$ cm$^3$ s$^{-1}$ and they (globally) slowly decrease with increasing $\Delta j_2$. The overall agreement is somewhat surprising, in particular for the B99 data set given the simplicity of the prescription. We note, however, that differences larger than a factor of 2 are observed for transitions with $\Delta j_2 > 2$ and, more generally, that the B99 set overestimates while the G93 set tends to underestimate the SACM rate coefficients.

It is now interesting to compare the efficiency of $H_2O$ relative to other colliders for exciting CO. In Fig. 3, the thermalized SACM rate coefficients for CO−$H_2O$ are compared to the corresponding data for CO−H (Yang et al. 2013), CO−He (Cecchi-Pestellini et al. 2002), CO−p-$H_2$, and CO−o-$H_2$ (Yang et al. 2010). These latter four sets of data were obtained from quantum close-coupling calculations combined with modern PES. Their accuracy at the state-to-state level is expected to be very good (about 20 per cent), as verified experimentally for CO−He and CO−$H_2$ (Carty et al. 2004; Chefdeville et al. 2015). We can first observe that, at 10 K, p-$H_2O$ and o-$H_2O$ are the most effective colliders with a rate coefficient for the transition $j_2 = 0 \to 1$ that is a factor of $\sim$2 larger than those for the other colliders. Atomic hydrogen is the less effective, with rate coefficients lower than $10^{-11}$ cm$^3$ s$^{-1}$. At larger temperatures, the $\Delta j_2$ dependence of the rate coefficients is found to be very different for $H_2O$ than for H and $H_2$: while the water rate coefficients slowly decrease with increasing $\Delta j_2$, a strong propensity rule with $\Delta j_2 = 2$ is observed for atomic and molecular hydrogen. As a result, the largest rate coefficients at 100 K are those of H and $H_2$ for the transition $j_2 = 0 \to 2$. For transitions with $\Delta j_2 > 2$, however, $H_2O$ is seen to be more than twice as effective as the other colliders. The magnitude of the rate coefficients for the excitation of CO by $H_2O$ is thus rather similar to that of other neutral colliders. The main difference is the lack of strong propensity rules and the relatively slow decrease of the rate coefficients with increasing $\Delta j_2$. This reflects mainly the larger potential well depth but also the fact that SACM calculations are not able to catch resonance and interference effects (Loreau et al. 2018a, 2018b). In particular, as discussed above, SACM calculations are expected to underestimate near-resonant rotational energy transfers.

We note, finally, that free electrons provide another source of CO rotational excitation in astronomical environments. Owing to the small dipole of CO (0.11 D), however, rate coefficients for electron-impact rotational excitation do no exceed $\sim 2 \times 10^{-8}$ cm$^3$ s$^{-1}$. This means that electrons compete with neutrals in exciting CO only when the electron-to-neutral number density ratio is larger than $\sim 10^{-2}$.

## 4 NON-LTE MODEL OF CO IN COMETS

In this section, we present a simple non-LTE model of CO excitation in a cometary coma. Our main objective is to assess the impact of the collisional rate coefficients on the predicted rotational populations of CO. We have chosen physical conditions corresponding to an *average* comet located at $R_h = 1$ au from the Sun with a total production rate from the nucleus $Q_{H_2O} = 1 \times 10^{29}$ s$^{-1}$, an expansion velocity $v_{exp} = 0.8$ km s$^{-1}$ and a neutral gas temperature $T_k$ in the range 10–100 K. Water is assumed to be the dominant neutral collider in the coma. The $H_2O$ density can be described by a standard isotropic Haser model (Haser 1957):

$$n_{H_2O}(r) = \frac{Q_{H_2O}}{4\pi r^2 v_{exp}} \exp\left(-r\frac{\beta_{H_2O}}{v_{exp}}\right), \quad (3)$$

where $r$ is the nucleocentric distance and $\beta_{H_2O}$ is the $H_2O$ photodissociation rate at $R_h = 1$ au. The coupled radiative transfer and statistical equilibrium (SE) equations are solved with the public version of the RADEX code using the large velocity gradient (LVG) approximation. The problem is treated as both local and steady state by running a grid of RADEX calculations covering a range of $H_2O$ densities. We thus assume that the physical processes driving the population are much faster than variations in physical conditions of the coma. Note that we also neglect CO photodissociation [the CO lifetime is about $5.3 \times 10^5$ s at $R_h = 1$ au for the active Sun (Huebner, Keady & Lyon 1992)] so that chemical processes (formation and destruction of CO) are omitted from the SE equations. This approach may not be valid over the whole coma and more elaborate and accurate non-LTE treatments exist in the literature (Zakharov et al. 2007; Yamada et al. 2018). We believe, however, that the main features of the collisional effects are well captured by our simple model.

The input parameters to RADEX are the kinetic temperature, $T_k$, the column density of CO, $N$(CO), the line width, $\Delta v$, and the density of the collider, here $n_{H_2O}$. Three kinetic temperatures were selected: 10, 50, and 100 K. The column density was

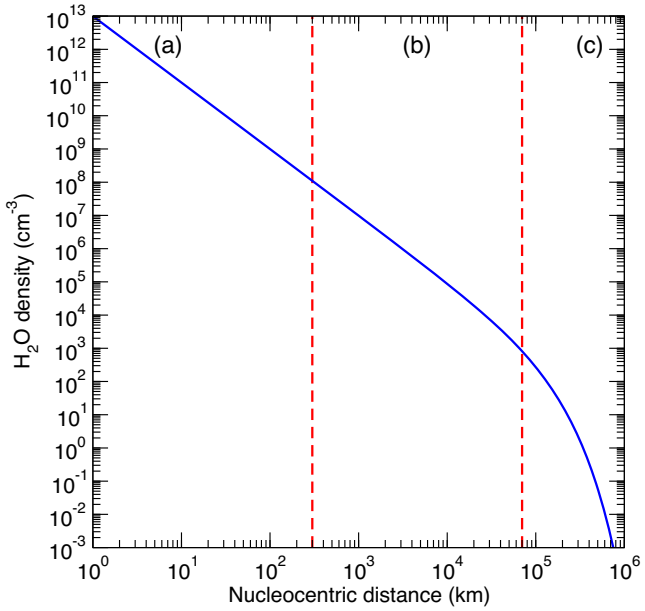


**Figure 4.** Coma density profile of $H_2O$ in the Haser's model. The photodissociation rate was taken as $\beta_{H_2O} = 1.042 \times 10^{-5}$ s$^{-1}$ from Zakharov et al. (2007). The dashed lines delineate, for a production rate $Q_{H_2O} = 1 \times 10^{29}$ s$^{-1}$, the three approximate density regimes: (a) LTE equilibrium, (b) non-LTE regime, and (c) fluorescence equilibrium. See text for details.

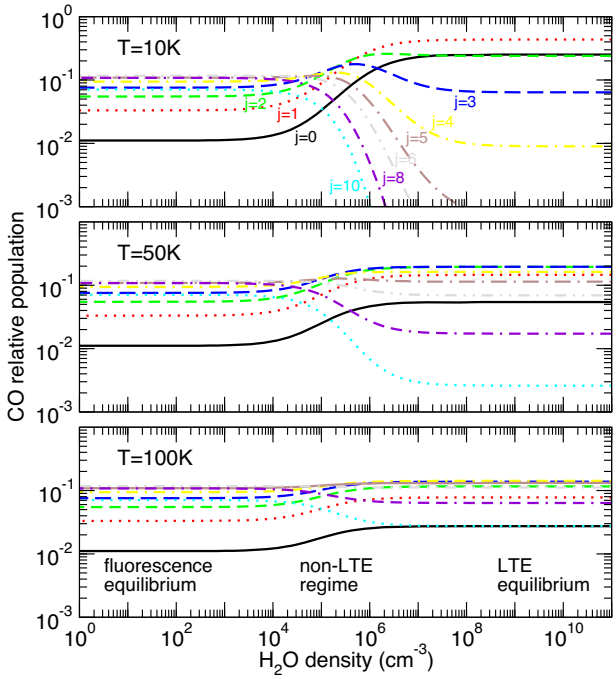


**Figure 5.** Level populations of CO ($j = 0 - 6$, 8, 10) as functions of $H_2O$ density for kinetic temperatures of 10, 50, and 100 K. The thermalized SACM rate coefficients are employed with an OPR of $H_2O$ fixed at 3.

fixed at $N(\mathrm{CO}) = 10^{14}$ cm$^{-2}$, which is the typical magnitude at $r \sim 1000$ km for a CO/$H_2O$ abundance ratio of ∼10 per cent (e.g. Lupu et al. 2007). We have checked, however, that the relative populations are not sensitive to the column density provided that $N(\mathrm{CO}) < 10^{16}$ cm$^{-2}$ (i.e. the lines are optically thin). The water density is varied in the large range $10^{-3}$–$10^{13}$ cm$^{-3}$ corresponding to nucleocentric distances between 1 and $10^6$ km in the Haser model, as plotted in Fig. 4. The line width is fixed at 1.6 km s$^{-1}$, i.e. $\Delta v = 2 \times v_{\mathrm{exp}}$. Finally, the background radiation field includes both the 2.73 K cosmic microwave background (CMB) and the Sun radiation. This latter contribution is taken as a diluted blackbody of 5770 K with the dilution factor $W = \Omega_S/4\pi$, where $\Omega_S \sim 6.79 \times 10^{-5}$ sr is the Sun solid angle seen at $R_{\mathrm{h}} = 1$ au.

Input data include the CO energy levels ($v_2$, $j_2$) ($v_2$ is the CO vibrational quantum number), the spontaneous emission Einstein coefficients and the collisional rate coefficients. Level energies and Einstein coefficients were taken from the HITRAN data base[1] (Gordon et al. 2017). Only the first excited vibrational level $v_2 = 1$ was taken into account because the solar excitation rate of $v_2 = 1$ is at least two orders of magnitude greater than those of $v_2 > 1$ (Crovisier & Le Bourlot 1983). Our model thus include the lowest 80 ro-vibrational levels of CO, i.e. up to level ($v_2$, $j_2$) = (1, 32) which lies 4148 cm$^{-1}$ above the ground-state (0, 0). Since our SACM rate coefficients are available for the lowest 11 rotational levels only, we had to extrapolate the collisional data above $j_2 = 10$. It should be noted, however, that the corresponding levels are negligibly populated (less than 1 per cent) at the investigated temperatures and the extrapolated collisional data play only a minor role in the SE equations. In practice, the *total* de-excitation rotational rate coefficients were simply fixed at $10^{-10}$ cm$^3$ s$^{-1}$ with an equal distribution among final levels and no temperature dependence.

[1] https://hitran.org/.

Similarly the *total* de-excitation vibrational rate coefficients were fixed at $10^{-13}$ cm$^3$ s$^{-1}$ (with again an equal distribution among final levels), as suggested by the CO($v_2 = 1$) − $H_2O$ quenching measurements of Wang, Gu & Kong (1999) performed at 300 K. Finally, for pure rotational transitions involving rotational levels $j_2 \leq 10$ within $v_2 = 1$, we adopted the corresponding rate coefficients within $v_2 = 0$. Rotational rate coefficients indeed depend only weakly on the vibrational state (Carty et al. 2004). This extrapolation procedure was used for the SACM, the B99 and the G93 collision data sets.

The population distribution of the CO rotational levels $j_2$ in $v_2 = 0$ is thus governed by the balance between the collision-induced transitions, the vibrational excitation ($v_2 = 0 \rightarrow 1$) by the solar infrared radiation field, the rotational excitation by the CMB radiation field and the radiative decay due to spontaneous emission. The results of our non-LTE model are presented in Fig. 5 where the population of levels $j_2$ is plotted as function of the $H_2O$ density for the selected kinetic temperatures 10, 50, and 100 K. The set of thermalized SACM rate coefficient is employed here with an OPR for $H_2O$ equal to 3. We can clearly observe the presence of three different regimes: the fluorescence equilibrium at low densities ($n_{H_2O} \lesssim 10^3$ cm$^{-3}$), the non-LTE regime in the range $10^3 \lesssim n_{H_2O} \lesssim 10^8$ cm$^{-3}$, and the LTE-regime at larger densities. Thus, for a production rate $Q_{H_2O} = 1 \times 10^{29}$ s$^{-1}$, LTE applies at $r \lesssim 300$ km, i.e. in the inner coma, while the fluorescence equilibrium distribution is completely established at $r \gtrsim 7 \times 10^4$ km (see Fig. 4). The non-LTE regime extends typically from 300 to 70 000 km, representing about 10 per cent of all CO molecules in the coma. We can notice in Fig. 5 that the non-LTE regime of densities does not significantly vary with temperature. In contrast, the LTE population distribution is very sensitive to the temperature: at 10 K significant populations (>1 per cent) are found only for $j_2 = 0$–3 while at 100 K all levels $j_2 = 0$–10 are occupied above 2 per cent.

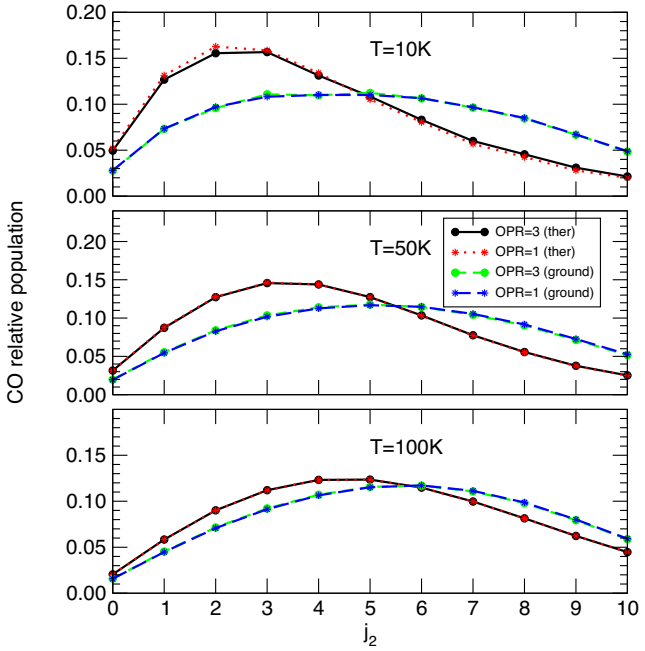


**Figure 6.** CO population distribution at a fixed $H_2O$ density of $1.9 \times 10^5$ cm$^{-3}$ for the three kinetic temperatures 10, 50, and 100 K. The SACM thermalized and ground-state rate coefficients are employed with an OPR of $H_2O$ equal to 1 and 3. See text for details.

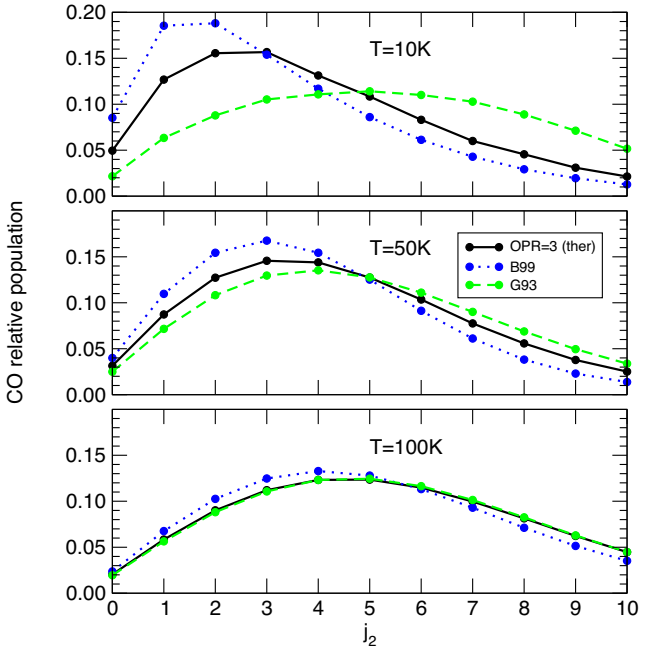


**Figure 7.** Same as Fig. 6. Three sets of collisional rate coefficients are employed: the thermalized SACM set with the OPR of $H_2O$ fixed at 3, the B99 set, and the G93 set. See text for details.

In the following, the $H_2O$ density is fixed at $n_{H_2O} = 1.9 \times 10^5$ cm$^{-3}$, which is representative of the non-LTE regime. The corresponding nucleocentric distance is $r \sim 7000$ km. In Fig. 6, the CO relative population is plotted as function of $j_2$ for the two sets of SACM rate coefficients (thermalized and ground-state) and for an OPR of $H_2O$ equal to 1 and 3. The OPR of $H_2O$ in comets is debated but values are generally comprised between 1 and 3, with a median equal to 2.9 (see Faure et al. 2019, and references therein). We first observe that the impact of the OPR of water is negligible, as expected from the small differences seen in Fig. 1. It can be also noticed that the thermalized SACM rate coefficients predict a more peaked distribution than the ground-state rate coefficients, with a greater population for low $j_2$ levels. The relative difference is found to reach ∼60 per cent at 10 K for $j_2 = 2$. This effect is due to pair correlations between CO and $H_2O$ transitions, as discussed in Section 3. Perhaps surprisingly, the influence of the $H_2O$ rotational distribution is found to be less important at higher temperature. In fact, this mainly reflects the LTE distributions which are closer to the fluorescence equilibrium distribution at 50 K and mostly 100 K than at 10 K, attenuating the impact of collisional data.

Finally, in Fig. 7 we compare the CO rotational populations as predicted by our thermalized SACM rate coefficients (with an OPR of $H_2O$ fixed at 3) and by the B99 and G93 rate coefficients. As in Fig. 6, the influence of collisional data is found to decrease with temperature, which again reflects the relative deviation between the LTE and the fluorescence equilibrium distribution. At 10 K, the uncertainties in collisional data have the largest impact with relative differences up to a factor of ∼3 for $j_2 = 1$. The B99 set overestimates while the G93 set underestimates the populations of levels $j_2 \lesssim 4$, which is consistent with the trend in the rate coefficients shown in Fig. 2. For levels with $j_2 > 4$, however, the reverse is observed, emphasizing the role of collisional transitions out of $j_2 > 0$.

In summary, using a simple non-LTE model of CO in standard cometary conditions, we have found that uncertainties in the collisional rate coefficients have a significant impact on the CO population distribution in the non-LTE regime ($n_{H_2O} \sim 10^5$ cm$^{-3}$). In particular, the CO rotational populations predicted by three different collisional data sets were found to differ by up to a factor of 3 at 10 K. Thanks to our SACM rate coefficients, we were also able to demonstrate that the $H_2O$ rotational distribution plays an important role, even at low temperature (due to correlated rotational energy transfers) while the OPR of $H_2O$ has an almost negligible influence.

## 5 CONCLUDING REMARKS

We have provided the first quantum rate coefficients for the rotational excitation of CO by p-$H_2O$ and o-$H_2O$. These rate coefficients were obtained by combining SACM calculations with a recent ab initio CO−$H_2O$ PES computed at the CCSD(T)-F12a/AVTZ level. Rotational transitions among the first 11 energy levels of CO and the first 8 energy levels of both p-$H_2O$ and o-$H_2O$ were considered. Two different sets of rate coefficients were obtained: one corresponding to p-$H_2O$ and o-$H_2O$ in their ground rotational state and one corresponding to thermal distributions of each nuclear-spin isomer. Correlated energy transfer in both CO and $H_2O$ was shown to be important while the differences between p-$H_2O$ and o-$H_2O$ were found to be small. Our set of 'thermalized' rate coefficients was compared to previous data from the literature and significant differences were observed. We also found that $H_2O$ is more effective than other colliders (H, He, and $H_2$) for exciting CO transitions with $\Delta j_2 > 2$. Finally, we have assessed the impact of the collision data on the CO population distribution in a cometary coma using a simple non-LTE model including collision-induced transitions, radiative pumping and radiative decay. We have found that the uncertainties in the collision data can affect the rotational populations by large factors at low temperature and at $H_2O$ densities $\sim 10^3$–$10^8$ cm$^{-3}$. In addition, the rotational distribution of $H_2O$ was found to play a significant role so that a consistent non-LTE model of CO excitation

should include a realistic (i.e. non-LTE) population distribution for $H_2O$. This in turn would require the knowledge of accurate $H_2O$-$H_2O$ rotational rate coefficients, which are lacking in the literature. On the other hand, the OPR of $H_2O$ was shown to have a negligible impact on the CO excitation, which removes one uncertainty from the interpretation of CO spectra.

Future studies will need to consider other linear targets such as CN, CS, $HCO^+$ as well as non-linear species such as $NH_3$, $H_2CO$, etc. colliding with both $H_2O$ and CO. The present SACM approach should be therefore extended to treat two non-linear polyatomic collision partners. We note that many data are available for the electron-impact rotational excitation of cometary molecules (e.g. Harrison, Faure & Tennyson 2013). Comparing the efficiency of electrons relative to neutrals ($H_2O$ and CO) will be very useful to distinguish between the different collisional non-LTE regimes in a comet ($H_2O$-, *e*-, or CO-dominated). Finally, we strongly encourage modellers to use the present CO−$H_2O$ data in any model of CO excitation in comets and, more generally, to use the ever-increasing amount of theoretical collision data available for astrophysical applications.

## SUPPORTING INFORMATION

Supplementary data are available at *MNRAS* online.

Please note: Oxford University Press is not responsible for the content or functionality of any supporting materials supplied by the authors. Any queries (other than missing material) should be directed to the corresponding author for the article.

## ACKNOWLEDGEMENTS

This research was supported by the Programme National 'Physique et Chimie du Milieu Interstellaire' (PCMI) of INSU, CNRS with INC/INP co-funded by CEA and CNES. Nicolas Biver, Jérémie Boissier and Lucas Paganini are acknowledged for very useful discussions.

## REFERENCES

Barclay A. J., van der Avoird A., McKellar A. R. W., Moazzen-Ahmadi N., 2019, Phys. Chem. Chem. Phys., 21, 14911
Bergeat A., Faure A., Morales S. B., Moudens A., Naulin C., 2020, J. Phys. Chem. A, 124, 259
Biver N., 1997, PhD thesis, Université Paris VII
Biver N. et al., 1999, AJ, 118, 1850
Bockelée-Morvan D., Crovisier J., Mumma M. J., Weaver H. A., 2004, in Festou M. C., Keller H. U., Weaver H. A., eds, The Composition of Cometary Volatiles, Comets II. University of Arizona Press, Tucson, p. 391
Buffa G., Tarrini O., Scappini F., Cecchi-Pestellini C., 2000, ApJS, 128, 597
Carty D., Goddard A., Sims I. R., Smith I. W. M., 2004, J. Chem. Phys., 121, 4671
Cecchi-Pestellini C., Bodo E., Balakrishnan N., Dalgarno A., 2002, ApJ, 571, 1015
Chefdeville S., Kalugina Y., van de Meerakker S. Y. T., Naulin C., Lique F., Costes M., 2013, Science, 341, 1094
Chefdeville S., Stoecklin T., Naulin C., Jankowski P., Szalewicz K., Faure A., Costes M., Bergeat A., 2015, ApJ, 799, L9
Crovisier J., Le Bourlot J., 1983, A&A, 123, 61
Dubernet M. L., Quintas-Sánchez E., 2019, Mol. Astrophys., 16, 100046
Faure A., Hily-Blant P., Rist C., Pineau des Forêts G., Matthews A., Flower D. R., 2019, MNRAS, 487, 3392
Gao Z., Loreau J., van der Avoird A., van de Meerakker S. Y. T., 2019, Phys. Chem. Chem. Phys., 21, 14033
Gordon I. E. et al., 2017, J. Quant. Spectrosc. Radiat. Transfer, 203, 3
Green S., 1993, ApJ, 412, 436
Harrison S., Faure A., Tennyson J., 2013, MNRAS, 435, 3541
Haser L., 1957, Bull. Soc. R. Sci. Liège, 43, 740
Huebner W. F., Keady J. J., Lyon S. P., 1992, Ap&SS, 195, 1
Kalugina Y. N., Faure A., van der Avoird A., Walker K., Lique F., 2018, Phys. Chem. Chem. Phys., 20, 5469
Kyrö E., 1981, J. Mol. Spectrosc., 88, 167
Liu Y., Li J., 2019, Phys. Chem. Chem. Phys, 21, 24101
Loreau J., Lique F., Faure A., 2018a, ApJ, 853, L5
Loreau J., Faure A., Lique F., 2018b, J. Chem. Phys., 148, 244308
Lupu R. E., Feldman P. D., Weaver H. A., Tozzi G.-P., 2007, ApJ, 670, 1473
Matrà L., Panić O., Wyatt M. C., Dent W. R. F., 2015, MNRAS, 447, 3936
Mengel M., Flatin D. C., De Lucia F. C., 2000, J. Chem. Phys., 112, 4069
Naulin C., Bergeat A., 2018, in Dulieu O., Osterwalder A., (eds), Cold Chemistry: Molecular Scattering and Reactivity Near Absolute Zero, The Royal Society of Chemistry, p. 92
Phillips T. R., Maluendes S., Green S., 1995, J. Chem. Phys., 102, 6024
Quack M., Troe J., 1975, Ber. Bunsenges, Phys. Chem., 79, 170
Rezac L., Kutepov A. A., Faure A., Hartogh P., Feofilov A. G., 2013, A&A, 555, A122
Wang B., Gu Y., Kong F., 1999, J. Phys. Chem. A, 103, 7395
Wiesenfeld L., Faure A., 2010, Phys. Rev. A, 82, 040702
Yamada T., Rezac L., Larsson R., Hartogh P., Yoshida N., Kasai Y., 2018, A&A, 619, A181
Yang B., Stancil P. C., Balakrishnan N., Forrey R. C., 2010, ApJ, 718, 1062
Yang B., Stancil P. C., Balakrishnan N., Forrey R. C., Bowman J. M., 2013, ApJ, 771, 49
Zakharov V., Bockelée-Morvan D., Biver N., Crovisier J., Lecacheux A., 2007, A&A, 473, 303

This paper has been typeset from a TEX/LATEX file prepared by the author.